DIFFERENTIAL SAR TOMOGRAPHY OF LARGE-SCALE WATER CONSERVANCY PROJECTS UNDER STEEP TERRAIN--THE CASE STUDY OF LAXIWA HYDROPOWER STATION

L. Li[1], L. Pang[1*],C. H. Li[1]

[1]School of Geomatics and Urban Spatial Informatics, Beijing University Of Civil Engineering And Architecture, No.15 Yongyuan Road, Daxing District, Beijing, China-2108570021074@stu.bucea.edu.cn,panglei@bucea.edu.cn,2108521519004@stu.bucea.edu.cn

KEY WORDS: Differential SAR Tomography, Permanent scatterer extraction, Deformation monitoring, Dam monitoring, Hydropower Engineering

ABSTRACT:

Differential SAR Tomography (D-TomoSAR), as an extension of InSAR technology, combines D-InSAR and TomoSAR technology to achieve imaging in the height-deformation rate (s-v) plane. It not only solves the layover problem of SAR imaging, but also obtains the height and deformation rate of each scatterer within the image element. The technique is currently mainly applied to complex scenes in urban areas where the layover problem is serious, and the layover effect also exists for hydropower plants with extremely steep slopes. In this paper, the Differential SAR Tomography technique is applied to the four-dimensional imaging of hydraulic engineering for the first time, taking the La Siwa hydropower station as an example. This experiment establishes the signal model based on permanent scatterer points, so interferometric processing and PS point selection should be performed to obtain the differential interferogram sequence and PS points in the region; the orthogonal matching pursuit (OMP) algorithm is selected for differential SAR tomography imaging processing to reconstruct the elevation-deformation rate backward scattering profile. The experiments use the 23-view TerraSAR-X satellite one-meter resolution time series image dataset for deformation monitoring of the Laxiwa hydropower dam in GuiDe County, Qinghai Province, China, and finally the resolution and reconstruction estimation performance are evaluated by theoretical analysis and application case study. A comparison with the traditional InSAR technique shows that the differential SAR tomography technique not only maintains the advantages of high resolution, but also significantly improves the probability of accurate reconstruction of scattered points, and achieves higher accuracy in estimating the deformation of hydropower dams. This paper mainly discusses the application of differential SAR tomography technology in water conservancy projects, hoping to provide reference and help for the future large-scale application of differential SAR tomography technology in hydroelectric dam deformation monitoring.

1. INTRODUCTION

With the booming development of hydropower construction in China, the quality level of dams is crucial, which determines the overall level of quality of water conservancy projects. Dam problems can bring disastrous consequences downstream, dam deformation monitoring is an important measure to ensure the safety of dams, is an indispensable task in the operation and management and post-maintenance. Dam safety monitoring is crucial to the construction and operation of dams, deformation monitoring, analysis and prediction is an important part of dam safety monitoring, timely understanding of the law of dam deformation, the completion of the dam deformation prediction can solve the safety risks in advance, so the importance of dam deformation monitoring is self-evident.

The traditional methods of dam deformation monitoring include GPS measurement, level monitoring and observation stakes, etc. These methods are mostly suitable for monitoring a certain location of the dam, but for the whole dam and slope monitoring, the traditional measurement methods appear to be powerless due to the large inspection area and long period. Although permanent scatterer (PS) and small baseline subset (SBAS), which are mainly time-series multi-baseline InSAR techniques, have greatly improved the accuracy and range of deformation monitoring, the scattering mechanism of these techniques is based on the dominant scatterer in the pixel, so when the buildings are very dense or the dam is located in a steep area, the scattering mechanism of these techniques is not suitable. However, the scattering mechanism of these techniques is based on the dominant scatterer in the pixel, and when the buildings are dense or the dam is located in a steep valley, a serious layover will occur, making a single radar resolution unit contain multiple scattering target signals from different heights. If these mixed signals cannot be distinguished effectively, accurate deformation monitoring cannot be performed(Pang, Gai, & Zhang, 2021a).

To address the problem that the above-mentioned methods cannot correctly solve the deformation variables due to the layover for high-resolution SAR data, the literature(Lombardini, 2003a) proposed differential SAR tomography (D-TomoSAR) as an extension of the InSAR technique, combining D-InSAR and TomoSAR technologies for imaging in the height-deformation rate (s-v) plane. This technique uses N aligned SAR images to recover the scattering coefficient distribution of the image elements in the s-v plane by a specific algorithm based on the magnitude and interference phase information of the image elements, which not only solves the layover problem of SAR imaging, but also obtains the elevation and deformation rate of each scatterer within the image elements(Aghababaee, Ferraioli, & Schirinzi, 2019a), the technique is currently mainly applied to complex scenes in urban areas with serious layover problem, and the layover effect also exists for hydropower plants with extremely steep side slopes. In this paper, taking the Laxiwa hydropower plant as an example, the differential SAR tomography technique is applied to four-dimensional imaging of water resources projects for the first time, which broadens the application scope of differential SAR tomography technique.

This experiment establishes the signal model based on permanent scatterer points, so interferometric processing and PS point selection should be performed to obtain the differential

* Corresponding author :panglei@bucea.edu.cn

interferogram sequence and PS points in this region; since the compressive sensing orthogonal matching pursuit algorithm (CS-OMP) minimizes the residuals by calculating the least squares solution and finally obtains the reconstructed signal with high accuracy, this paper selects the orthogonal matching pursuit (OMP) algorithm for differential SAR tomography imaging processing to reconstruct the elevation-deformation rate backward scattering profile(Fornaro, Reale, & Serafino, 2008a). The experiments use the 26-view TerraSAR-X satellite one-meter resolution time series image dataset to monitor the deformation of the Laxiwa hydropower dam in GuiDe County, Qinghai Province, China, and finally evaluate the resolution and reconstruction estimation performance through theoretical analysis and application case studies. It is found that the differential SAR tomography technique not only maintains the advantages of high resolution, but also substantially improves the probability of accurate reconstruction of scattering points, and achieves higher accuracy of hydroelectric dam deformation estimation(Zhu & Bamler, 2011a). This paper mainly discusses the application of differential SAR tomography technology in water conservancy projects, and hopes to provide reference and help for the future large-scale application of differential SAR tomography technology in hydroelectric dam deformation monitoring.

2. STUDY AREA DATA AND PREPROCESSING

2.1 Study area data

Laxiwa Hydropower Station is located in Laxiwa Town, Qinghai Province, China, on the main stream of the Yellow River in Qinghai Province, and is the second large step-up hydropower station in the upper section of the Yellow River, which is located in a higher altitude area, with an altitude of about 3,200 meters above sea level, in the high altitude zone of the Qinghai-Tibet Plateau. Laxiwa Hydropower Station is the largest hydropower station and clean energy base on the Yellow River, as well as the hydropower station with the highest dam, the largest installed capacity and the largest power generation capacity in the Yellow River basin. The geographical location is shown in Figure 1:

(a) (b)

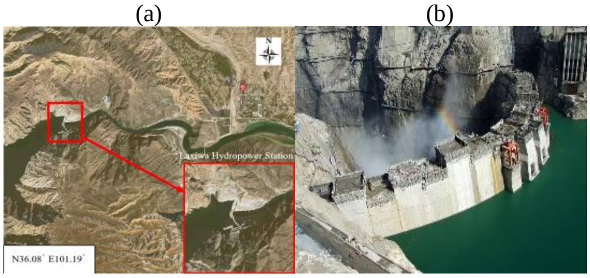

Fig.1 （a）Hydroelectric Power Station Location，（b）Hydroelectric Power Station Overview

Table 1 Detailed stataement of SAR data

Items	Parameters
Data Source	TerrSAR-X
Imaging mode	Stripmap,descending orbit
Polarization mode	HH
Number of views	23
Coverage area	La Xiva town
Time span	2015.12.21-2018.01.07
Wavelength	0.031m
Incident Angle	26.601 °
The Center slant distance （the master image）	557428.0921m
Range Resolution	0.455m
Azimuth Resolution	0.855m

The SAR data used in this experiment come from the satellite-based TerrSAR-X/TanDEM-X platform with high-resolution and wide-format imaging capability, working in X-band, and the initial image data are .xml format files, which can be converted to .slc format (Single Look Complex, SLC) by using the professional SAR processing software Gamma.The SAR data details are shown in Table 1.

2.2 Preprocessing

Data preprocessing mainly includes master image selection, image alignment and cropping, spatial and temporal baseline estimation, and amplitude correction. The selection of the master image generally selects the image with the centered time baseline and spatial baseline, so as to reduce the spatial decoherence and temporal decoherence effects and ensure the quality of the interferogram; Image alignment is based on fitting an alignment polynomial with intensity correlation information, and an alignment accuracy of 0.01 pixels has been achieved in the study area of the La Xiwa hydropower plant; The cropping of the image must ensure that the entire study area is cropped, for example, Figure 2 shows the main image intensity map and the corresponding optical remote sensing image of the La Xiwa hydropower plant (Ge, Bamler, Hong, & Zhu, 2021a)。

(a) (b)

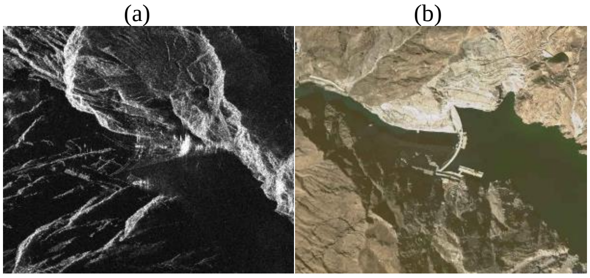

Fig.2 （a）SAR images of the study area,（b）Optical images of the study area

The spatial-temporal baseline estimation uses the satellite high-precision orbit data to calculate the vertical baseline between each auxiliary image and the master image separately, and the time baseline calculates the time difference according to the acquisition date and converts the unit to year, and the final baseline data is organized as shown in Table 2。

Table 2 Data list of time and spatial perpendicular baseline

Image Serial Number	Date of imaging	Time Baseline (year)	Spatial Baseline(m)
1	2015/12/21	-0.8740	51.2284
2	2016/01/12	-0.8137	1.7290
3	2016/03/07	-0.6630	12.4902
4	2016/04/09	-0.5726	65.3896
5	2016/05/12	-0.4822	-55.7527
6	2016/06/14	-0.3918	55.4476
7	2016/07/17	-0.3014	-77.7760
8	2016/08/08	-0.2411	-45.8032
9	2016/08/30	-0.1808	41.8775
10	2016/10/02	-0.0904	-125.5880
11	2016/11/04*	0.0000	0.0000
12	2016/12/07	0.0904	-55.1782

13	2017/01/09	0.1808	-94.1276
14	2017/02/11	0.2712	-70.3624
15	2017/03/16	0.3616	-234.3367
16	2017/04/18	0.4521	-244.0170
17	2017/05/21	0.5425	-119.0347
18	2017/06/23	0.6329	72.7903
19	2017/07/26	0.7233	-123.0691
20	2017/08/28	0.8137	-205.7589
21	2017/11/02	0.9945	164.1232
22	2017/12/05	1.0849	-43.3109
23	2018/01/07	1.1753	-232.9067

Note: marked with * for the master image

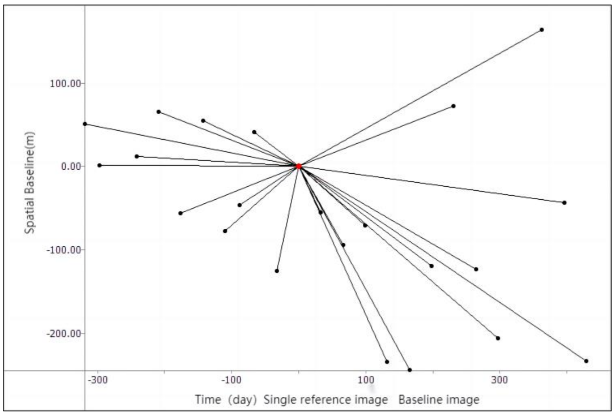

Fig.3 Spatial-Temporal Baseline Plot

Finally, an amplitude correction is needed for each SLC image, divided by the average amplitude of each image, which is used to remove the overall relative deviation between images, which will directly affect the subsequent amplitude departure index method candidate PS points.

3. DIFFERENTIAL SAR TOMOGRAPHY FRAMEWORK

The overall technical process is shown in Fig 4. After the pre-processing of the SAR image sequence is completed, interferometric processing and PS point selection are carried out to prepare for the differential SAR tomography process, and then the tomography-deformation rate backward scattering profile reconstruction is carried out using the OMP algorithm to finally obtain the 3D information and deformation information of the target (Zhu et al., 2019a).

3.1 Interference processing and ps point selection

Firstly, interferometric processing is carried out. The cropped image of the study area is interfered with the master image in turn to generate an interferogram sequence, and then an external DEM is introduced for geocoding, which is converted to the SAR coordinate system and aligned with the image. Finally, the geocoded external DEM and orbital parameter information are used to generate simulated topographic phases, and finally a differential interferogram sequence with topographic and flat earth phases removed is obtained (Fornaro, Reale, & Serafino, 2009a).

PS point selection is very important, it is a key step in the process of differential SAR tomography. By selecting the PS point, the low coherence region can be avoided and the spatial and temporal decoherence problems can be solved effectively. This experiment mainly adopts the amplitude dispersion index method for PS point selection, which mainly uses the statistical distribution of amplitude to select stable PS points (Ge & Zhu, 2019a)，The PS points are selected by analyzing the time series composed of echo amplitudes. The main rule is to select the points with larger MSR values, where $MSR = \frac{\mu}{\sigma}$,μ and σ are the mean and standard deviation of the amplitude of each image element of N SAR images respectively, and the amplitude departure index method is simple to calculate, suitable for processing multi-scene image data and for processing large blocks of data in blocks, as shown in Figure 5 for the PS points of this experimental selection area.

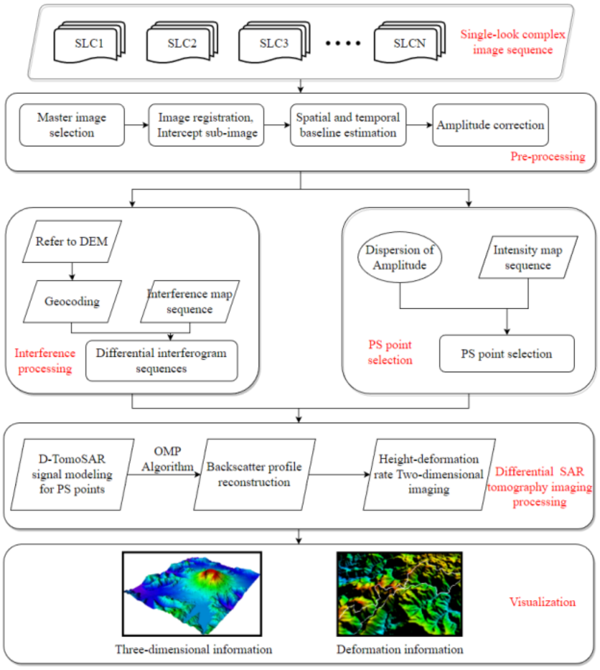

Fig.4 Overall technical flow chart

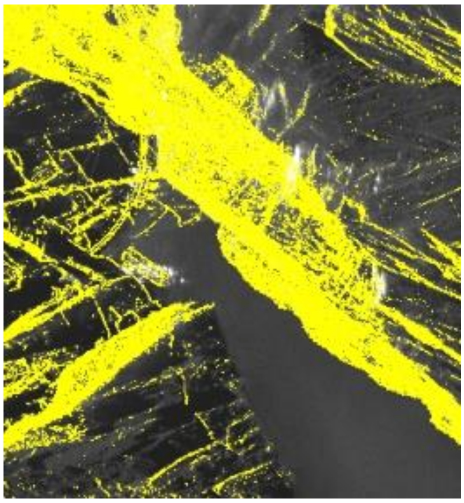

Fig.5 LaXiwa Hydropower Station PS Point

3.2 D-TomoSAR system mode

D-TomoSAR framework deeply integrates the principles of TomoSAR and D-InSAR, and since TomoSAR ignores the temporal dimension, D-InSAR extracts only the (possibly average) height of a single scatterer within an image pixel. D-TomoSAR is an extension of scatterer separation in D-InSAR, solving the problem of layover in high-resolution SAR image features (Montazeri, Zhu, Eineder, & Bamler, 2016a).

We assume that M repetitive flight trajectory data of single-channel SAR over the region of interest are processed, and M SAR single-view complex images are obtained after two-dimensional compression in the azimuth-distance direction, one image with a more centered spatial and temporal baseline is selected as the main image, and the other images are aligned and deskewed with the main image as the standard to obtain a complex sequence of image azimuth-range resolution units, which is expressed as

$$g_m = \int_{-s_{max}}^{s_{max}} a(s) exp\left(j \frac{4\pi}{\lambda} \frac{b_m}{r}\right) exp(j\varphi_m) ds \qquad (1)$$
$$m = 1,2,\cdots,M$$

Where $[-s_{max}\ ,\ s_{max}]$ is the slant range vertical span;$a(s)$is the radar scattering characteristic function of the target;λ is the wavelength;$r$is the slant range of the master image; b_m is the vertical baseline of the aerial over image and the master image;φ_m is the phase direction of the slant range deformation rate direction at the sampling point of the tomographic direction (Serafino, Soldovieri, Lombardini, & Fornaro, 2005a).Under the linear deformation rate model $\varphi_m = -\frac{4\pi}{\lambda} t_m v(s)$,if we let $\xi_m = \frac{2b_m}{\lambda r}$, $\eta_m = \frac{2t_m}{\lambda}$, $\gamma(s,v) = a(s)\delta(v - v(s))$, then equation (1) can be written in the following form

$$g_m = \int_{-s_{max}}^{s_{max}} \int_{-v_{max}}^{v_{max}} a(s,v) exp(j2\pi\xi_m s) exp(j2\pi\eta_m v) ds dv \quad (2)$$
$$m = 1,2,\cdots,M$$

where $[v_{-max}\ , v_{max}]$ is the deformation rate span; ξ_m and $\eta_m$are the spatial and temporal frequencies, respectively;v is the slant range deformation rate direction sampling point; $\delta(v - v(s))$is the Dirac function(Xiang & Bamler, 2010a). According to equation (2), the observed data of D-TomoSAR is the two-dimensional joint spectrum of the radar scattering characteristic function in the elevation -velocity direction, and the scattering function value of the target signal is derived by the inversion of specific imaging algorithm, and the position of the scattering point in the elevation and the size of the velocity are determined according to the position of the function value to achieve four-dimensional imaging.(Lombardini & Cai, 2019a)。

3.3 Compressive sensing

The unknown discrete signal $\Upsilon = [\gamma_1, \gamma_2, \cdots, \gamma_M]^T$, and the signal γ can be expressed as a linear combination of a set of standard orthogonal bases $y_m, m = 1,2,\cdots,M$

$$\gamma = \sum_{m=1}^{M} \alpha_m y_m = \boldsymbol{Y\alpha}$$

Where $\boldsymbol{Y} = [y_1, y_2, \cdots, y_M]$,$\boldsymbol{\alpha} = [\alpha_1, \alpha_2, \cdots, \alpha_M]^{\boldsymbol{T}}$, if the non-zero element in $\boldsymbol{\alpha}$ is K or the element decays according to a certain order of magnitude power,and K<<M,then γ is said to be K-sparse(Lombardini & Pardini, 2012a). Suppose that the $M \times 1$-dimensional observation g of γ is obtained through the observation matrix $\Phi_{M\times N}(M \ll N)$, $g = \Phi\gamma = \Theta\alpha$,where $\Theta = \Phi Y$, becomes the sensing matrix. It follows from compressive sensing theory that if the signal γ is K-sparse on $\boldsymbol{Y}$, when the sensing matrix Θ satisfies the RIP condition, the signal can be reconstructed with high accuracy by a small number of projections of γ on Φ. The reconstruction equation is as follows

$$\hat{\gamma} = argmin\|Y^{-1}f\|_0 \quad subject\ to \quad g = \Phi\gamma \qquad (3)$$

Since (3) is an NP-hard problem, solving the minimum l_1 parametric problem for the following equation will yield a n equivalent solution

$$\hat{\gamma} = argmin\|Y^{-1}f\|_1 \quad subject\ to \quad g = \Phi\gamma \qquad (4)$$

The differential tomography formula can be further written in matrix form, $g_{M\times 1} = \Phi_{M\times N} \cdot \gamma_{N\times 1}$, where $g = [g_1, g_2, \cdots, g_M]^T$, $\gamma = [a(s_1, v_1), \cdots, a(s_1, v_q), \cdots, a(s_p, v_1), \cdots, a(s_p, v_q)]^T$,and the observation matrix Φ is denoted as

$$\Phi = \begin{bmatrix} exp(j2\pi\xi_1 s_1)exp(j2\pi\eta_1 v_1), \cdots, exp(j2\pi\xi_1 s_1)exp(j2\pi\eta_1 v_q), \cdots, exp(j2\pi\xi_1 s_p)exp(j2\pi\eta_1 v_1), \cdots, exp(j2\pi\xi_1 s_p)exp(j2\pi\eta_1 v_q) \\ exp(j2\pi\xi_2 s_1)exp(j2\pi\eta_2 v_1), \cdots, exp(j2\pi\xi_2 s_1)exp(j2\pi\eta_2 v_q), \cdots, exp(j2\pi\xi_2 s_p)exp(j2\pi\eta_2 v_1), \cdots, exp(j2\pi\xi_2 s_p)exp(j2\pi\eta_2 v_q) \\ \vdots \qquad \vdots \qquad \vdots \qquad \vdots \\ exp(j2\pi\xi_M s_1)exp(j2\pi\eta_M v_1), \cdots, exp(j2\pi\xi_M s_1)exp(j2\pi\eta_M v_q), \cdots, exp(j2\pi\xi_M s_p)exp(j2\pi\eta_M v_1), \cdots, exp(j2\pi\xi_M s_p)exp(j2\pi\eta_M v_q) \end{bmatrix}$$

In this paper, we use the compressive sensing technique approach of OMP algorithm for 2D signal reconstruction, which is more suitable for compressive sensing framework and performing signal inversion than the traditional MP algorithm (Qian, Wang, Shi, & Zhu, 2022a)。The specific steps of OMP algorithm are as follows:

1、Input matrices A, b and the number of variables to be picked k 。Initialize the residual $r_0 = b$, the orthogonal projection matrix $P_0 = 0$, the subspace index set $S = \emptyset$, and the recovery signal $x = 0$.

2、Calculate $i = argmax_i|A_i^T r_k|$,put i into the set S,that is $S = S \cup \{i\}$。

3、Calculate $P_k = A_S(A_S^T A_S)^{-1} A_S^T, r_k = (I - P_k)b$。

4、Repeat step 2 and step 3 k times.

5、Calculate $x_s = (A_S^T A_S)^{-1} A_S^T b$, and get the value of the element in x whose corresponding position is S.

6、Return x.

4. RESULT AND ANALYSIS

In order to verify the applicability and accuracy of the new method proposed in this paper for dam deformation monitoring, differential SAR tomography was performed on the Laxiwa Hydropower Dam in Qinghai Province as an example (high-resolution data set and satellite parameter information, incidence angle and oblique distance of each data, spatial time baseline, resolution and other details are shown in 2.1). As shown in Figure 6, the deformation monitoring results of the top of the LaXiwa hydropower dam can be seen from the figure, the overall point cloud outline of the top of the hydropower plant is clearly visible, but due to the SAR side-looking imaging mechanism, part of the structural parts on the back side facing the sensor may not be monitored, which is also a major shortcoming of this deformation monitoring technology, but this shortcoming can be fully compensated by the joint monitoring of the ascending-descending data. The overall deformation rate of the top structure of LaXiwa Hydropower Station is relatively small and stable, with the majority of scatterers deforming in the range of 0~-1.5mm. This deformation level is acceptable in the post-deformation maintenance of the dam.

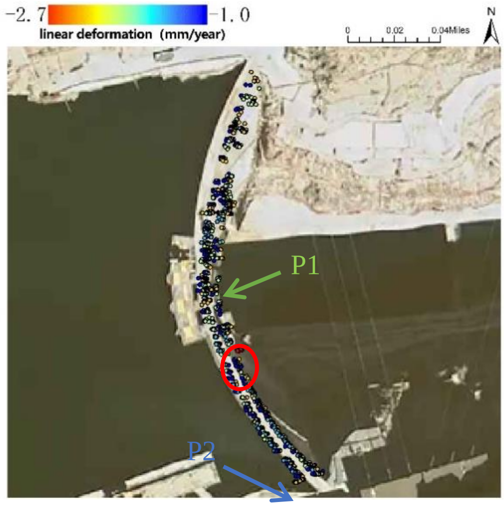

Fig.6 3D point cloud and deformation rate map of the top of the hydropower dam

The deformation rate of 8 scatterer points in Figure 6 is significantly higher than the rest of the points. After repeatedly confirming that it is not the excessive deformation of the dam structure, but that these points are distributed in an electrical control room building on the dam, which is in line with the deformation law and the dam is relatively stable as a whole. There is no large deformation, and the deformation rate is in the range of 0~-1.5mm, which not only maintains the same deformation rate accuracy as the traditional InSAR technology, but also can obtain high-precision 3D point cloud data, solving the problem of the lack of elevation resolution capability of the traditional InSAR technology.

As shown in Figures 7 and 8, the deformation rates of the two strong scattering points at the top of the dam for each time period relative to the master image of 20161104, P1 scattering point is located in the middle of the dam, due to the force of the water pressure P1 will have a small deformation in the downstream direction, but each stage deformation is uniform and stable in the normal range; P2 scattering point is located in the south side of the dam slope out so the deformation rate here is smaller, and the annual deformation rate is between -1 ~ 1mm/year range, which leads to the conclusion that the dam body is very stable.

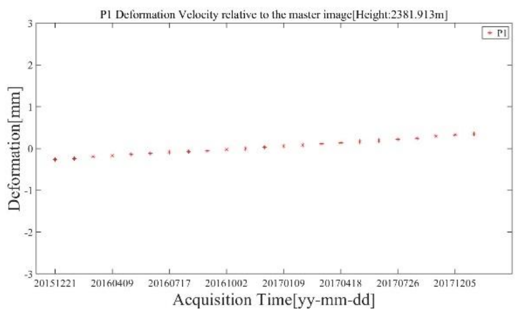

Fig.7 Deformation rate sequence of scatterer P1

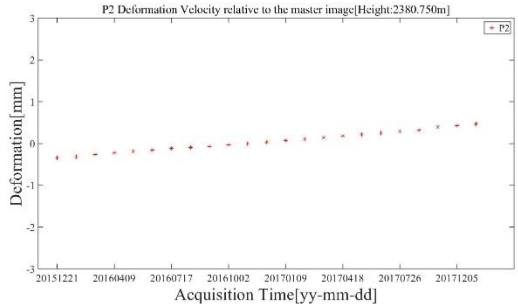

Fig.8 Deformation rate sequence of scatterer P2

As Figure 9 and Figure 10 show the four-dimensional imaging of the overall deformation rate of the dam in two different directions, the X,Y,Z coordinates represent the azimuth-range-height imaging, and the color represents the deformation rate. From the figure, we can also see that the overall structure of the dam is very healthy, only a few scatterer points at the top of the dam deformation rate exceeds the value of the dam safety range, the specific reasons have been explained above, here will not repeat.

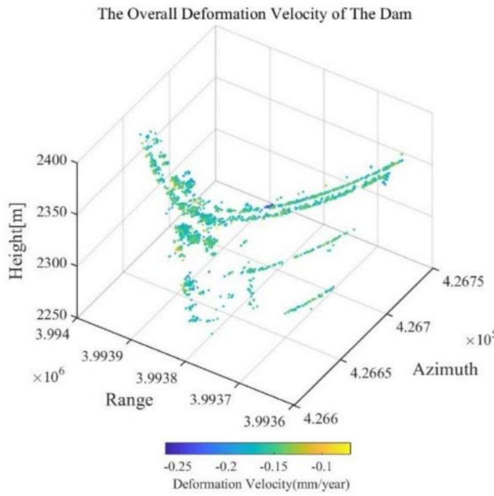

Fig.9 Dam overall deformation rate angle1

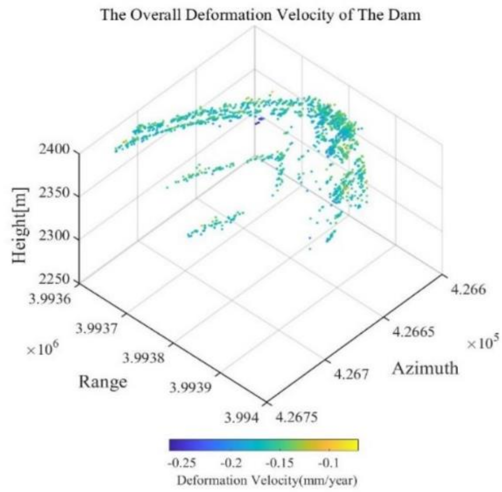

Fig.10 Dam overall deformation rate angle2

Next, the accuracy verification is carried out, but in practical applications, the verification of linear deformation variables requires a long time span (two and a half years in this case) of fixed-point horizontal monitoring devices to continuously collect information, which is time-consuming and difficult to cover a large area; only the elevation is the easiest and most direct effective verification set, so in this experiment, the accuracy of the results is mainly verified by the elevation.

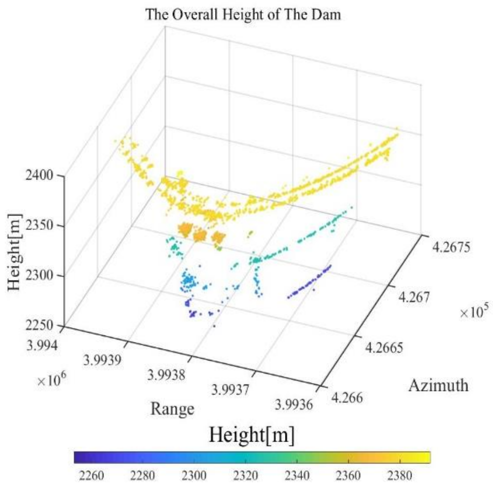

Fig.11 Dam 3D information angle 1

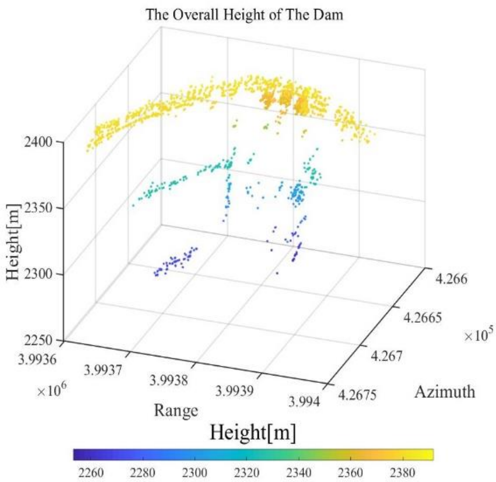

Fig.12 Dam 3D information angle 2

First of all, qualitative verification is carried out, and it can be seen from Fig. 11 and Fig. 12 that the inverse elevation fits well with the actual features, and the shapes of buildings are clearly visible, which can indicate that the elevation is basically correct. There is a conversion problem here, because the projection plane of the 90m DEM external data we chose for the differential SAR tomography is not the same as the geodetic level for measuring elevation in China, and the difference between the two planes is 70m, so the average actual height of the top of the dam should be about 2451m, and it is known that the elevation of the top of the dam is 2452m after consulting the data.

Then quantitative verification is performed. For the dam, we have the elevation data obtained by traditional techniques to assist in the verification, and the elevation data are geocoded and projected, then converted to the D-TomoSAR coordinate system, and then the scatter plot shown in Figure 13 is drawn by the closest point pair, and the results show that the two elevations are basically the same, and the fitted standard deviation is within 1m, which illustrates the specified requirements of the accuracy Of the 4-D inversion results.

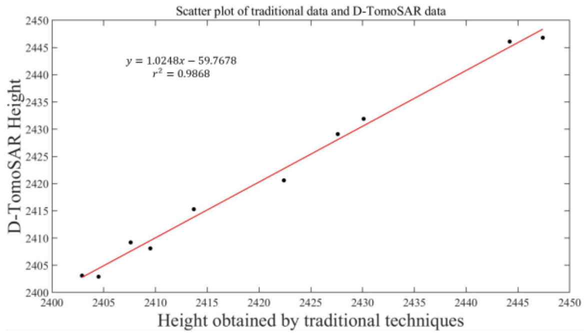

Fig.13 Traditional measurement and D-TomoSAR elevation scatter plot

5. CONCLUSION

Based on the advanced D-TomoSAR technology, this paper focuses on the field of dam deformation monitoring and strives to explore the potential and value of D-TomoSAR technology in the field of dam monitoring. This paper mainly uses Matlab to implement the D-TomoSAR algorithm and conducts a detailed study of the Laxiwa Hydropower Station in Laxiwa Town, GuiDe County, Qinghai Province using 23 scenes of TerraSAR real data to verify the high practical value of D-TomoSAR technology in dam deformation monitoring. The experimental investigation of the dam shows that the overall deformation condition of the dam is relatively stable, and each structural part is relatively healthy, with linear deformation mostly distributed in the range of 0~-1.5 mm/year, abnormal deformation of individual parts or beyond the theoretical deformation range, but not a threat to the overall stability of the dam, This study provides a reference for the further application of D-TomoSAR technology in the field of dam deformation monitoring in the future. However, there are some shortcomings in this study. Firstly, the SAR side-looking imaging mechanism makes the information on the back side of the antenna missing, and the combination of ascending and descending orbital data can be considered in the future to make up for the current deformation deficiency and to monitor the dam more comprehensively; Secondly, the current dam deformation information is limited to the line of sight, only a component of the real deformation of the dam, can not be a comprehensive access to dam deformation information, the future can consider mathematical modeling, numerical simulation, etc. to study the real three-dimensional deformation information of the features.

6. ACKNOWLEDGEMENTS

First of all, I would like to sincerely thank my advisor, Lei Pang, for her guiding comments and helpful suggestions on my dissertation. I am deeply grateful to her for her help in completing this dissertation. Secondly, I should pay a high tribute to Mr. Chonghui Zhang, whose profound knowledge of English sparked my love for this beautiful language and whose serious attitude showed me how to learn English. I would also like to express my deep gratitude to my friends who invested a lot of time and effort in writing my thesis. Finally, I would also like to thank my parents for their constant support and encouragement.

REFERENCES

Aghababaee, H., Ferraioli, G., & Schirinzi, G. (2019a). Differential SAR Tomography Reconstruction Robust to Temporal Decorrelation Effects. *Ieee Transactions on Geoscience and Remote Sensing, 57*(11), 9071-9080. doi:10.1109/tgrs.2019.2924738

Fornaro, G., Reale, D., & Serafino, F. (2008a, 7-11 July 2008). *4D SAR Focusing: A Tool for Improved Imaging and Monitoring of Urban Areas.* Paper presented at the IGARSS 2008 - 2008 IEEE International Geoscience and Remote Sensing Symposium.

Fornaro, G., Reale, D., & Serafino, F. (2009a). Four-Dimensional SAR Imaging for Height Estimation and Monitoring of Single and Double Scatterers. *Ieee Transactions on Geoscience and Remote Sensing, 47*(1), 224-237. doi:10.1109/TGRS.2008.2000837

Ge, N., Bamler, R., Hong, D. F., & Zhu, X. X. (2021a). Single-Look Multi-Master SAR Tomography: An Introduction. *Ieee Transactions on Geoscience and Remote Sensing, 59*(3), 2132-2154. doi:10.1109/tgrs.2020.3002945

Ge, N., & Zhu, X. X. (2019a). Bistatic-Like Differential SAR Tomography. *Ieee Transactions on Geoscience and Remote Sensing, 57*(8), 5883-5893. doi:10.1109/tgrs.2019.2902814

Lombardini, F. (2003a, 21-25 July 2003). *Differential tomography: a new framework for SAR interferometry.* Paper presented at the IGARSS 2003. 2003 IEEE International Geoscience and Remote Sensing Symposium. Proceedings (IEEE Cat. No.03CH37477).

Lombardini, F., & Cai, F. (2019a). Generalized-Capon Method for Diff-Tomo SAR Analyses of Decorrelating Scatterers. *Remote Sensing, 11*(4). doi:10.3390/rs11040412

Lombardini, F., & Pardini, M. (2012a). Superresolution Differential Tomography: Experiments on Identification of Multiple Scatterers in Spaceborne SAR Data. *Ieee Transactions on Geoscience and Remote Sensing, 50*(4), 1117-1129. doi:10.1109/TGRS.2011.2164925

Montazeri, S., Zhu, X. X., Eineder, M., & Bamler, R. (2016a). Three-Dimensional Deformation Monitoring of Urban Infrastructure by Tomographic SAR Using Multitrack TerraSAR-X Data Stacks. *Ieee Transactions on Geoscience and Remote Sensing, 54*(12), 6868-6878. doi:10.1109/TGRS.2016.2585741

Pang, L., Gai, Y. F., & Zhang, T. (2021a). Joint Sparsity for TomoSAR Imaging in Urban Areas Using Building POI and TerraSAR-X Staring Spotlight Data. *Sensors, 21*(20). doi:10.3390/s21206888

Qian, K., Wang, Y. Y., Shi, Y. L., & Zhu, X. X. (2022a). gamma-Net: Superresolving SAR Tomographic Inversion via Deep Learning. *Ieee Transactions on Geoscience and Remote Sensing, 60*. doi:10.1109/tgrs.2022.3164193

Serafino, F., Soldovieri, F., Lombardini, F., & Fornaro, G. (2005a, 29-29 July 2005). *Singular value decomposition applied to 4D SAR imaging.* Paper presented at the Proceedings. 2005 IEEE International Geoscience and Remote Sensing Symposium, 2005. IGARSS '05.

Xiang, Z. X., & Bamler, R. (2010a, 25-30 July 2010). *Compressive sensing for high resolution differential SAR tomography - the SL1MMER algorithm.* Paper presented at the 2010 IEEE International Geoscience and Remote Sensing Symposium.

Zhu, X. X., & Bamler, R. (2011a). Let's Do the Time Warp: Multicomponent Nonlinear Motion Estimation in Differential SAR Tomography. *IEEE Geoscience and Remote Sensing Letters, 8*(4), 735-739. doi:10.1109/LGRS.2010.2103298

Zhu, X. X., Dong, Z., Yu, A. X., Wu, M. Q., Li, D. X., & Zhang, Y. S. (2019a). New Approaches for Robust and Efficient Detection of Persistent Scatterers in SAR Tomography. *Remote Sensing, 11*(3). doi:10.3390/rs11030356